water

MDPI

Article

Flash Flood Potential Analysis and Hazard Mapping of Wadi Mujib Using GIS and Hydrological Modelling Approach

Moayyad Shawaqfah [1], Yazan Ababneh [2], Alhaj-Saleh A. Odat [3], Fares AlMomani [4,*], Alaa Alomush [5], Fayez Abdullah [5] and Hatem H. Almasaeid [1]

[1] Civil Engineering Department, College of Engineering, Al Al-Bayt University, P.O. Box 130040, Mafraq 25113, Jordan; mshawaqfah@aabu.edu.jo (M.S.)
[2] Civil Engineering Department, College of Engineering, Yarmouk University, P.O. Box 3030, Irbid 22110, Jordan; yazan.ababneh@yu.edu.jo
[3] Department of Renewable Energy Engineering, College of Engineering, Al Al-Bayt University, P.O. Box 130040, Mafraq 25113, Jordan; saleh.odat@aabu.edu.jo
[4] Department of Chemical Engineering, College of Engineering, Qatar University, Doha P.O. Box 2713, Qatar
[5] Civil Engineering Department, College of Engineering, Jordan University of Science and Technology, P.O. Box 3030, Irbid 22110, Jordan; alaa_omoush95@yahoo.com (A.A.); fabdulla@just.edu.jo (F.A.)
* Correspondence: falmomani@qu.edu.qa

Abstract: Jordan experienced flash floods that resulted in numerous fatalities and injuries. This research focuses on identifying the Wadi Mujib's flash flood potential zones and evaluating their potential magnitude. In this work, hydrological models were developed by integrating GIS settings with HEC-HMS software (V. 4.11). The hydrological model for Wadi Mujib is simulated in this research by means of the Soil Conservation Service (curve number method) while using rainfall data from 1970 to 2022. The results show that the optimum curve number values (CN) were 78.5 at normal antecedent moisture content. Additionally, in order to aid in the decision-making process for flash flood warnings, a flash flood potential index (FFPI) was also introduced based on four main physiographic parameters (slope, land use, plant cover, and soil texture) ranging from 1 to 10. The accumulative chart's FFPI threshold, which indicates the areas with the highest potential for flash floods, was set at 95% or above. The FFPI threshold was chosen using the accumulative chart of FFPI, which shows that the FFPM threshold value is 7 and covers 13.39% of the study area.

Keywords: flash flood; Wadi Mujib; flash flood guidance; hazardous flooding; hydrological factors; HEC-HMS; GIS

check for updates

Citation: Shawaqfah, M.; Ababneh, Y.; Odat, A.-S.A.; AlMomani, F.; Alomush, A.; Abdullah, F.; Almasaeid, H.H. Flash Flood Potential Analysis and Hazard Mapping of Wadi Mujib Using GIS and Hydrological Modelling Approach. *Water* **2024**, *16*, 1918. https://doi.org/10.3390/w16131918

Academic Editors: Athanasios Loukas and Chang Huang

Received: 29 September 2023
Revised: 9 December 2023
Accepted: 12 January 2024
Published: 5 July 2024

Copyright: © 2024 by the authors. Licensee MDPI, Basel, Switzerland. This article is an open access article distributed under the terms and conditions of the Creative Commons Attribution (CC BY) license (https://creativecommons.org/licenses/by/4.0/).

1. Introduction

Flash floods are measured to be the maximum hazardous form of flooding, characterized by intense and heavy rainfall occurring within a brief timeframe [1]. These floods can occur shortly after precipitation or even in a matter of minutes, displaying an exceptionally high-flow velocity that renders them highly unpredictable and capable of causing catastrophic damage [2]. Hydrological factors play a crucial role in the incidence of flash floods, with precipitation concentration and duration being the primary variables of significance [3]. Urbanization, alongside various other factors, contributes to the expansion of impervious surface areas, leading to sudden rises in water levels during flash flood events [4].

Over the previous two decades, climate change has had a substantial influence on water resources worldwide, and especially in Jordan, causing unexpected and sudden flash floods [5]. As highlighted in Jordan's Third National Communication report to the United Nations Framework Convention on Climate Change (UNFCCC), flash floods are considered a serious threat to many people in Jordan, and have taken many lives over the past years [5]. For instance, in 1963, 23 individuals lost their lives due to flash floods

in Wadi Musa. Furthermore, on 21 October 2018, a devastating incident at the Dead Sea claimed the lives of 21 people, including 14 students who were on a school trip [6].

In the field of hydrology, the rainfall-runoff model has played a crucial role in assessing, mapping, and predicting flash floods across diverse study areas [7]. The curve number method has been widely adopted as a loss method in numerous studies, either within a conceptual lumped model or a semi-distributed model [7,8]. This approach offers simplicity in estimating flow or flood volume and is compatible with various software packages. Among these, the HEC-HMS software has gained popularity for developing rainfall-runoff models [9–11]. Many studies have leveraged GIS environments along with the HEC-GeoHMS (V. 10.1) extension to prepare basins and export catchment parameters to the HEC-HMS software, while others have manually entered the necessary parameters [5,12–14].

Moreover, extensive research has been devoted to understanding the physical mechanisms and underlying factors that contribute to the occurrence of flash floods. Several aspects influence flash floods, including the amount and timing of precipitation, as well as basin characteristics like slope, terrain, and surface conditions [7,15]. Researchers have also used rainfall-runoff models to evaluate the likelihood of flash floods using detailed spatial data [16]. Flash flood guidance (FFG) is employed to determine the precipitation threshold required within a specific timeframe to trigger flooding in small streams [16]. The curve number (CN) method is frequently used in semi-distributed models to calculate the flow volume in each sub-basin [1]. Within GIS environments, maps are generated and categorized based on flow volume [17]. Furthermore, catchment characteristics such as soil type, drainage density, land use, and slope can be incorporated to produce hazard maps as additional indicators of flash floods [18–21]. These factors can be weighted using the Analytical Hierarchical Process (AHP) or expert opinions to further enhance their relevance [22]. In 2010, Smith proposed an alternative method known as the "flash flood potential index" (FFPI) to map flash floods without relying on hydrological models [23]. This approach takes into account four essential physiographic elements: slope, land utilization, vegetation coverage, and soil texture. These factors are assigned rankings ranging from 1 (indicating low runoff contribution) to 10 (indicating high runoff contribution) based on their hydrological response [8,17,24]. Soil textures are categorized based on their infiltration rates [25], while the curve number (CN) values are used to determine the land use factor [1,11,16]. The vegetation coverage is inversely associated with the risk of flash floods, as determined by the interception process [26,27]. The slope factor, on the other hand, is inversely proportional to the time of concentration (the time of discharge), which increases the flow velocity and escalates the risk of flash floods [26,27]. In GIS environments, maps are generated by overlaying various factors to depict the potential for flash floods at different levels [28–34]. These levels are categorized from 1 (indicating the lowest potential) to 10 (indicating the highest potential) [28–34].

The objective of this research is to evaluate the flash flood potential and magnitude in Wadi Mujib, Jordan. The article focuses on integrating GIS settings with HEC-HMS software to develop hydrological models. The Soil Conservation Service curve number method is employed to simulate the hydrological response of Wadi Mujib. Additionally, a flash flood potential index (FFPI) grid is introduced to aid in flash flood warning decision-making. The FFPI grid integrates key physiographic elements including slope, land use, vegetation cover, and soil texture, which are classified and ranked based on their hydrological response. This study aims to generate a hazard map, known as the Flash Flood Potential Map (FFPM), using GIS analysis and the aforementioned parameters. The methodology involves processing Digital Elevation Model (DEM) data, developing hydrological models, calibrating and validating the models, conducting frequency analysis of rainfall data, and estimating flash flood flows at different return periods.

The remnant of this article is systematized as follows. Section 2 will provide the methodology and datasets used in this research. Section 3 will present the results and analysis of the findings. Finally, key findings will be summarized in Section 4.

2. Datasets and Methodology

2.1. Study Area Topology and Specifications

In the heart of Jordan lies the precisely studied Mujib Basin, strategically positioned in the central region, showcased in Figure 1. Defined by the Palestinian grid coordinates spanning from 205 to 297 east and 10 to 146 north, this expansive basin covers an extensive area of approximately 6397 km^2. Noteworthy for its hydrological significance, it comprises two major catchment areas: the Wadi Mujib catchment, covering around 4297 km^2, and the Wadi Wala catchment, spanning about 2100 km^2. Geographically, it is flanked to the west by the Dead Sea catchment, to the north by the Zarqa Basin, to the east by the Azraq Basin, and to the south by the Jafr Basin.

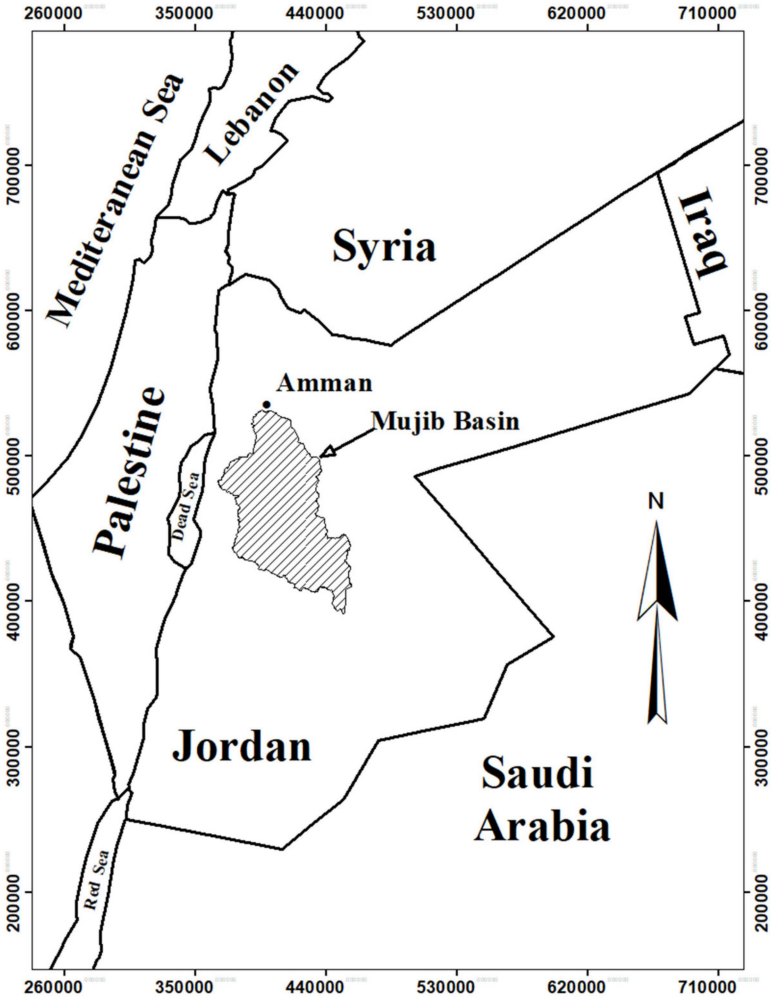


Figure 1. Study area location.

This region is enveloped by the Al-Karak, Amman, and Ma'an governorates, encapsulating an area of 4297 km^2. The altitude within this captivating landscape fluctuates between 1269 and −326 a.m.s.l., as depicted in Figure 2. The terrain, predominantly comprising 88.9% bare soil and rocks, undergoes a harmonious transformation with 10.9% adorned by vegetation, including pastures and forests. The residual area is allocated for urban development, as displayed in Figure 3. A closer examination of the soil texture distribution unfolds, revealing that loam constitutes a substantial 60.7%, followed by clay at 23.6%, and the remaining spectrum encompasses diverse soil types, as vividly portrayed in Figure 4. The vegetation cover unfolds in Figure 5, with approximately 6.8% dedicated to dense forests, while the rest exhibits low density or unveils the natural allure of bare soil. This comprehensive exploration offers a nuanced understanding of the Mujib Basin and

Wadi Mujib, laying the groundwork for insightful hydrological evaluations and ecological analyses.

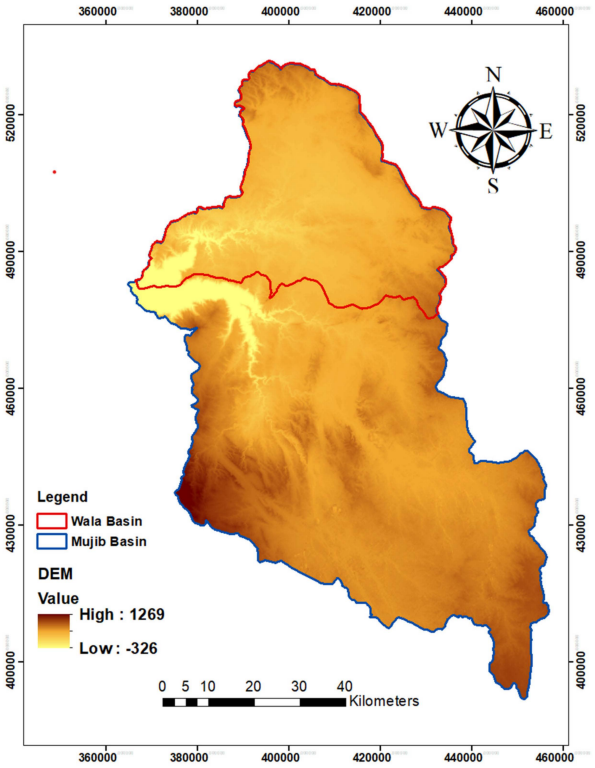


Figure 2. Wadi Mujib topography.

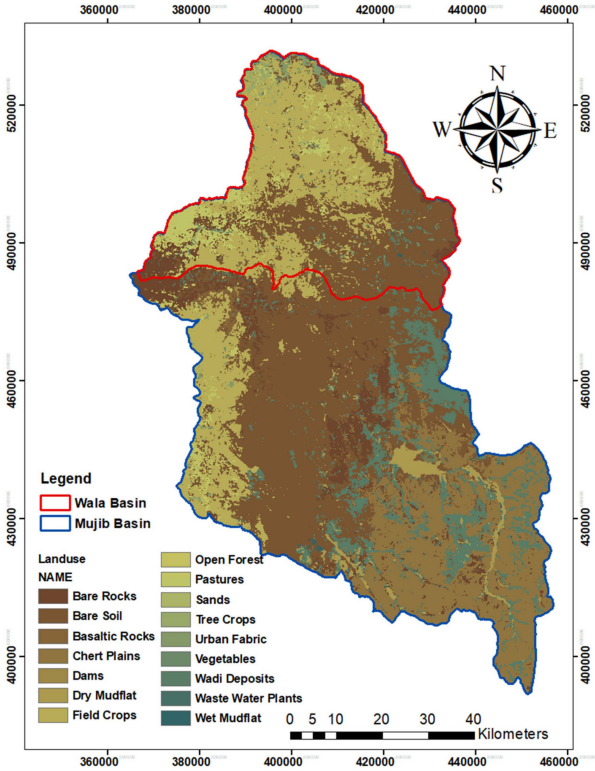


Figure 3. Land use/land cover of Wadi Mujib.

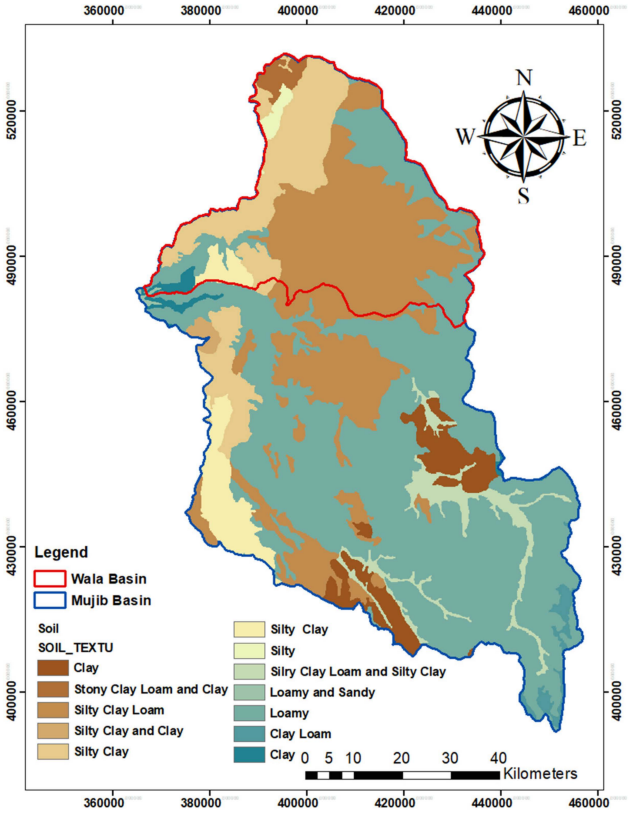


Figure 4. Soil texture of Wadi Mujib.

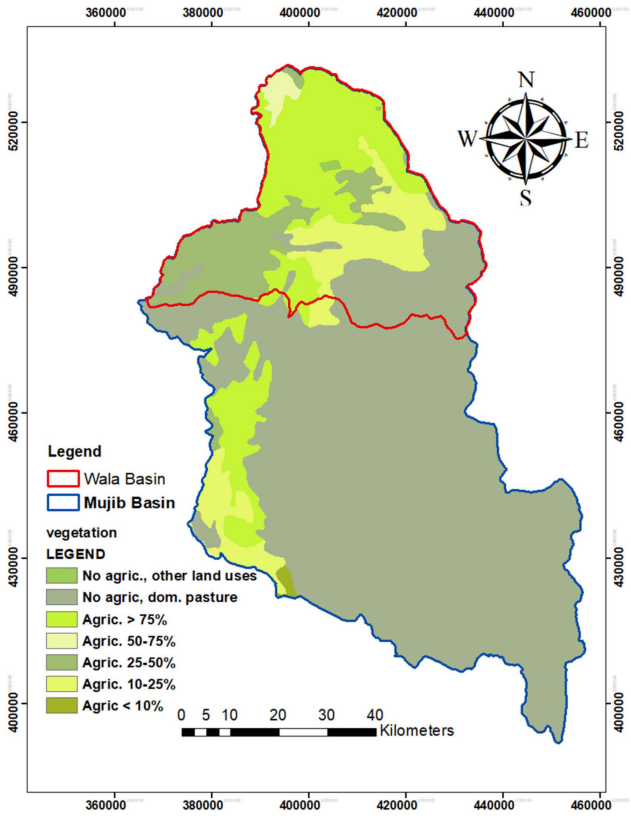


Figure 5. Vegetation cover of Wadi Mujib.

2.2. Hydrology Data of Study Area

The climate within the Mujib Basin exhibits distinctive trends, influenced by a north-south and west-east orientation. The northern and western mountainous regions experience a Mediterranean climate, while the eastern and southern hills lean towards arid to semi-arid conditions. The primary contributor to rainfall is the Mediterranean air mass, particularly during the winter season spanning from October to April, impacting key climate factors like atmospheric pressure, temperature, relative humidity, and sunshine hours along this macroscopic trend [14].

For comprehensive hydrological calculations, data from seven meteorological stations with robust datasets were harnessed for this study. These stations, namely Na'our, Madaba, Wadi Wala, Rabbah, Hassan, Al Jiza, and Qatrana, were strategically chosen. The mean temperature at each station reflects its elevation, with Wadi Wala station exhibiting higher figures due to its lower elevation. The average annual minimum and maximum temperatures across all stations stand at 10.2 °C and 22.6 °C, respectively.

Monthly variations in mean temperature, relative humidity, wind speed, and cloudiness ratio for these stations are intricately detailed in Table 1. It provides a comprehensive overview of climatic conditions throughout the year, offering insights into the dynamic nature of the Mujib Basin. The locations of these meteorological stations are visually represented in Figure 6.

Table 1. Monthly average metrological data for Mujib Basin.

Factor	Station	Oct.	Nov.	Dec.	Jan.	Feb.	Mar.	Apr.	May	Jun.	Jul.	Aug.	Sep.	Mean
1. Mean Temperature °C	Na'our	18.9	13	9.2	7	8.1	10.3	14.2	18.1	21.3	22.7	22.4	21.1	15.5
	Madaba	19.7	14.1	9.7	7.7	9	11.3	15.2	19.1	22.2	24.1	23.5	22.3	16.5
	Wadi Wala	21.8	16.5	11.7	10.5	11.1	13.5	18.1	21.3	24.1	25.8	25.3	24.2	18.7
	Rabbah	19.6	14	9.6	7.6	8.9	11.2	15.3	19.5	22	23.3	22.9	21.5	16.3
	Hassan	18.6	12.7	8.5	6.3	7.6	10.4	14.8	18.9	21.6	23.3	23.2	21.6	15.6
	Al Jiza	18.4	13	9	7.4	9	11.1	15.4	18.9	21.6	23	22.2	21	15.8
	Qatrana	20	13.9	9.8	8.1	9.2	12.2	16.6	18.1	21.9	23.7	21.3	20	16.2
2. Mean Relative Humidity (%)	Na'our	51	55	75	77	74	70	55	46	40	46	48	51	57.3
	Madaba	49	51	72	71	74	66	54	42	47	44	47	45	55.2
	Wadi Wala	50	44	67	67	69	63	51	38	42	42	46	48	52.3
	Rabbah	52	57	70	73	61	65	54	46	44	49	51	57	56.6
	Hassan	46	55	63	64	65	59	44	41	45	42	43	47	51.2
	Al Jiza	55	59	74	73	74	71	57	50	50	53	56	59	60.9
	Qatrana	62	65	71	77	71	70	63	57	57	55	59	61	64.0
3. Mean Wind Speed (m/s)	Na'our	2.2	2.8	2.2	3	3.2	3.1	3.6	3.2	3.3	3.7	3.7	3.1	3.1
	Madaba	2.4	3.9	3.2	3	3.4	3.1	3.3	2.7	2.5	3.1	3.2	2.6	3.0
	Wadi Wala	2.2	2.9	2.8	2	2.7	2.5	2	2.7	2.5	2.7	2.9	3.3	2.6
	Rabbah	2.1	2.6	2.4	2.6	2.9	3.1	2.9	2.5	2.4	2.9	2.4	2.3	2.6
	Hassan	2.6	3.2	3.2	3.8	4.2	4.2	4.1	3.4	3.4	3.5	3.1	2.6	3.4
	Al Jiza	2.2	2.5	2.7	2.6	3.3	3.7	3.5	3.2	3.1	3.8	2.8	2.2	3.0
	Qatrana	1.8	2.5	2.3	2.4	3.2	2.8	3.5	3.2	3.6	3.4	3.3	2.4	2.9
cloudness ratio (n/D)	Na'our	0.81	0.63	0.58	0.59	0.62	0.62	0.64	0.78	0.96	0.94	0.98	0.96	0.8
	Madaba	0.78	0.55	0.46	0.57	0.45	0.52	0.56	0.7	0.95	0.93	0.98	0.97	0.7
	Wadi Wala	0.84	0.71	0.66	0.68	0.6	0.63	0.72	0.78	0.96	0.94	0.95	0.98	0.8
	Al Jiza	0.87	0.77	0.63	0.64	0.63	0.62	0.68	0.77	0.96	0.96	0.98	0.96	0.8
	Rabbah	0.76	0.74	0.6	0.72	0.59	0.62	0.69	0.73	0.83	0.81	0.83	0.83	0.7
	Hassan	0.8	0.79	0.7	0.69	0.67	0.72	0.7	0.8	0.87	0.88	0.87	0.85	0.8
	Qatrana	0.87	0.73	0.66	0.6	0.58	0.65	0.75	0.78	0.84	0.9	0.9	0.89	0.8

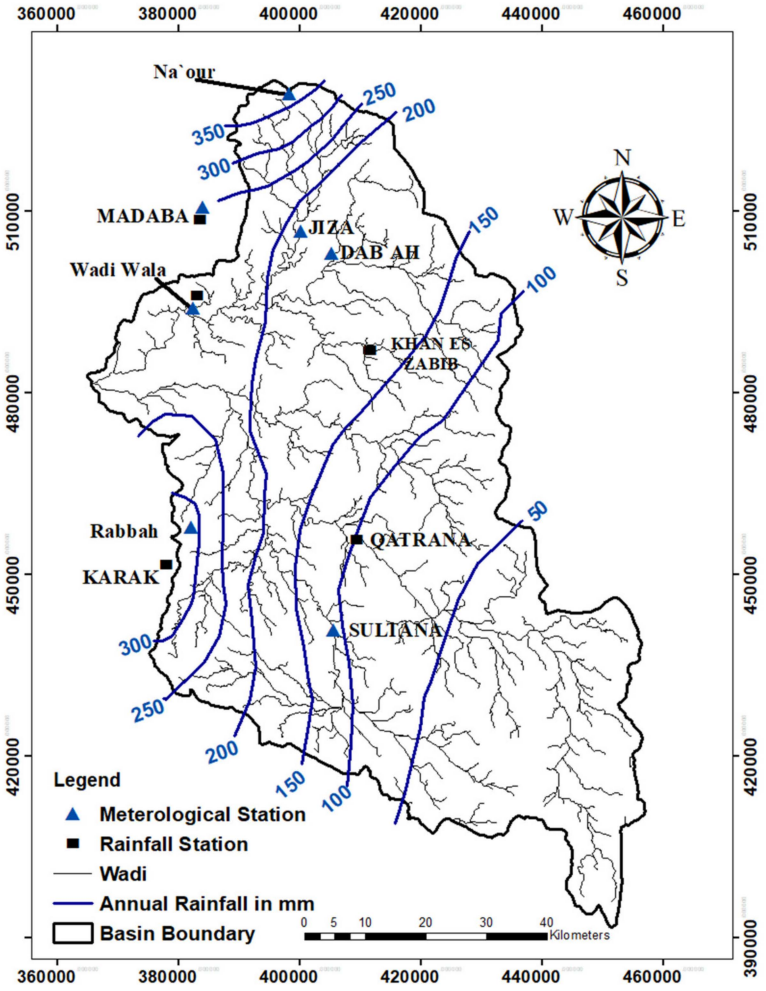


Figure 6. Isohyet and location map of metrological and rainfall station.

Further analysis reveals that mean monthly relative humidity ranges between 40% and 55% for eight months and fluctuates from 60% to 75% for the crucial rainfall months of December to March. The wind run, influenced by elevation, demonstrates varying strengths, ranging from 2.0 m/s to 4.2 m/s in higher elevated areas and 2.0 m/s to 3.3 m/s in lower elevated areas. Wind directions predominantly oscillate between northwest and southeast, with occasional shifts to easterly and southwesterly directions. The westerly and northerly winds carry humidity, while the easterly and southerly winds are dry. This nuanced climatic analysis forms a pivotal foundation for understanding Mujib Basin's hydrological dynamics.

Moreover, the annual precipitation across the region exhibits a range from 50 mm to 500 mm, with a distinct bias towards the western and northern sectors of the Mujib Basin, illustrated in Figure 6. The cumulative annual rainfall over the entire Mujib catchment is approximately 866 million cubic meters (MCM), boasting an average annual precipitation of 131 mm. Within this, the Wadi Mujib section accounts for around 497 MCM, with an average rainfall of 111 mm, while the Wadi Wala segment records about 369 MCM, featuring a higher average rainfall of 174 mm. This comprehensive overview of the annual rainfall patterns and noteworthy wet years forms a crucial backdrop for understanding the hydrological dynamics of the Mujib Basin. It is worth noting that the rainfall data and streamflow data for the selected catchments were acquired from the Ministry of Water and Irrigation in Jordan.

2.3. Soil Texture and Vegetation Coverage of Study Area

To conduct a thorough analysis of the study area's characteristics, detailed information on soil texture, land use, and vegetation coverage was gathered. Topsoil maps, acquired from the Ministry of Agriculture at a resolution of 30 m × 30 m, provided insights into seven distinct soil types, as outlined in Table 2. The SRTM Digital Elevation Model (DEM) Data, with a resolution of 30 m, were sourced from the USGS Earth Explorer website [35,36].

Table 2. Soil texture classifications [25].

No.	Soil Texture
1	Silty Clay Loam
2	Clay Loam
3	Silty Clay
4	Clay
5	Loamy
6	Silty Clay and Clay
7	Silty Clay Loam and Silty Clay

Additionally, the LandUse map, also obtained from the Ministry of Agriculture at a resolution of 30 m × 30 m, proved to be a precise and comprehensive resource [37]. It classifies the land into 17 categories, as detailed in Table 3. Vegetation coverage information was extracted from satellite images with a resolution of 30 m × 30 m. Categorized into 10 classes based on vegetation density, the details are presented in Table 4. This multi-faceted dataset lays the foundation for a comprehensive understanding of the study area's topography and ecological features.

Table 3. Land use classifications [25,37].

No.	Land Use Classify	No.	Land Use Classify
1	Pastures	10	Dams
2	Vegetables	11	Urban Fabric
3	Sands	12	Open Forest
4	Tree Crops	13	Wadi Deposits
5	Basaltic Rocks	14	Bare Soil
6	Bare Rocks	15	Field Crops
7	Chert Plains	16	Waste Water Plants
8	Dry Mudflat	17	Quarries
9	Wet Mudflat		

Table 4. Vegetation cover classifications [37].

No.	Vegetation Cover
1	20–29%
2	40–49%
3	50–59%
4	60–69%
5	70–79%
6	80–89%

2.4. Methodology

Initially, the processing of the Digital Elevation Model (DEM) involved a meticulous application of GIS tools, with a specific focus on leveraging the ArcHydro and HEC-GeoHMS extensions. These tools were instrumental in delineating the basin and establishing its precise boundary within the defined study area [9,38–47]. Building upon the methodologies outlined by [1,9], this step aimed to ensure a comprehensive and accurate representation of the geographic features.

Following the basin delineation, the next crucial phase involved the creation of a curve number grid. This grid was meticulously formulated by integrating information from the land use map and soil map. The process involved the adept utilization of the CN grid tool within the GIS environment and the HEC-GeoHMS extension. This sophisticated approach allowed for the initial estimation of the average curve number specific to Wadi Mujib for the context of this study. The integration of land use and soil data ensured a nuanced and context-specific representation of hydrological characteristics.

To quantify precipitation accurately within the study area, the Thiessen Polygon method was employed. This methodological choice involved utilizing the Thiessen Polygon tool within the ArcGIS software (V. 10.1). The tool facilitated the creation of polygons based on the percentage area covered by each meteorological station within the basin. The Thiessen Polygons were meticulously constructed by calculating the proportional contribution of each station to the overall basin area. The mathematical representation of this process can be articulated as follows:

$$P_B = \sum_{i=1}^{n} \frac{P_i \times A_i}{A} \quad (1)$$

where P_i is the rainfall of station i, A_i is the area of polygon covered by station i, A is the total area of that basin, and n is the number of the polygons of the basin.

The conclusive phase of this study involved the intricate simulation of the hydrological model utilizing the HEC-HMS program, a sophisticated software developed under the purview of the U.S. Army Corps of Engineers (USACE). In order to fashion a comprehensive model, a suite of pivotal parameters, including the basin area, curve number value, and lag time, were meticulously curated. Additionally, the selection of the loss technique and transformation method played a crucial role in shaping the robustness of the model. The seamless transfer of critical parameters from the ArcGIS software to the HEC-HMS software was orchestrated through the seamless integration of the HEC-GeoHMS extension. This intricate process ensured that the geospatial data, encompassing vital components essential for accurate modeling, flowed seamlessly between the GIS environment and the hydrological modeling software. The meticulous exportation of parameters was paramount in establishing a reliable foundation for the subsequent simulation endeavors.

Following the preparatory phase, the model underwent a rigorous calibration and verification process. This phase was meticulously executed using a comprehensive dataset derived from storm events spanning the temporal expanse between 1970 and 2022. The calibration model, strategically formulated to refine the model's accuracy, judiciously incorporated two-thirds of the recorded data relating to precipitation and runoff. This thoughtful partitioning of data facilitated an in-depth calibration process, ensuring that the hydrological model could adeptly capture the intricate dynamics of storm events in the study area. Concomitantly, the remaining one-third of the dataset was deliberately reserved for the pivotal stage of model validation. This approach, characterized by a distinct separation of data for calibration and validation purposes, bolstered the robustness of the hydrological model. The validation process rigorously scrutinized the model's performance against real-world storm events, providing a stringent assessment of its reliability and predictive capabilities. Moreover, areal precipitation, a pivotal component of the hydrological model, was calculated with precision using the Thiessen Polygon method. This spatially distributed estimation of precipitation within the study area was integral to the accurate representation of hydrological responses in the model. The Thiessen

Polygon method, characterized by its nuanced approach to precipitation delineation, further attested to the meticulous detailing inherent in the methodology. The final step of this study involved a comprehensive and detailed simulation of the hydrological model, underpinned by the HEC-HMS program. This endeavor, intricately woven with the integration of GIS tools and data, culminated in a meticulously calibrated and validated model, equipped to simulate storm events with a temporal scope spanning over five decades. The judicious partitioning of data for calibration and validation, coupled with the precise calculation of areal precipitation, attested to the methodological rigor employed in ensuring the accuracy and reliability of the hydrological model in the dynamic context of the study area.

The FFPI method relies on four types of spatial resolution data presented in raster format: basin slope, vegetation cover, land use, and soil texture. These maps were categorized according to the classifications shown in Table 5 using GIS environments. Moreover, the flash flood potential map for the study area was generated using the raster calculator tool in the ArcGIS software. The objective of this step was to create a map that spatially depicts the potential for flash floods by employing Equation (1). The coefficients used in Equation (2) were obtained through personal communication with an expert. The FFPI method relies on four types of spatial resolution data presented in raster format: basin slope, vegetation cover, land use, and soil texture. These maps were categorized according to the classifications shown in Table 4 using GIS environments. Subsequently, the flash flood potential map for the study area was generated using the raster calculator tool in the ArcGIS software. The objective of this step was to create a map that spatially depicts the potential for flash floods by employing Equation (2). The coefficients used in Equation (2) were obtained through personal communication with an expert.

$$FFPI = [(1.51 * M) + (1.32 * L) + (1.16 * S) + (1.02 * V)]/5 \quad (2)$$

where M is the slope, L is the land use, S is the soil, and V is the vegetation cover [6].

Table 5. Flash flood index values for the table attribute of each parameter.

FFPI Value	Slope	Land Use	Vegetation Cover	Soil
1	0–3%	Dead Sea/Dams/Wastewater Plants	90–100%	Water/Alluvial
2	3–6%	Chert Plains/Wet Mudflat/Wadi Deposits	80–89%	Sand
3	6–9%	Closed Forest	70–79%	Sandy Loam
4	9–12%	Vegetables/Dry Mudflat/Open Forest/Field Crops	60–67%	Silty Loam, Loamy Sand
5	12–15%	Deciduous Forest	50–59%	Silt/Organic Matter
6	15–18%	Pastures/Tree Crops	40–49%	Loam
7	18–21%	Bare Soil	30–39%	Sandy Clay Loam, Silty Clay Loam
8	21–24%	Basaltic Rocks/Bare Rocks/Granite/Quarries	20–29%	Silty Clay, Clay Loam, Sandy Clay
9	24–27%	Sands	10–19%	Clay
10	More than 27%	Urban Fabric	0–9%	Bed Rock/Impervious

3. Results and Discussion

In adopting a comprehensive methodology that leveraged the synergies of Geographic Information System (GIS) and HEC-HMS software, this study embarked on the intricate task of simulating hydrological models. The dynamic capabilities offered by the ArcHydro and

HEC-GeoHMS extensions, integral components of the versatile ArcGIS software, played a pivotal role in the precise delineation of the study areas' basins. A visual representation of the topographical features, encapsulated in Figure 7, showcased the generated slope—an indispensable parameter for calculating the lag time within the study area.

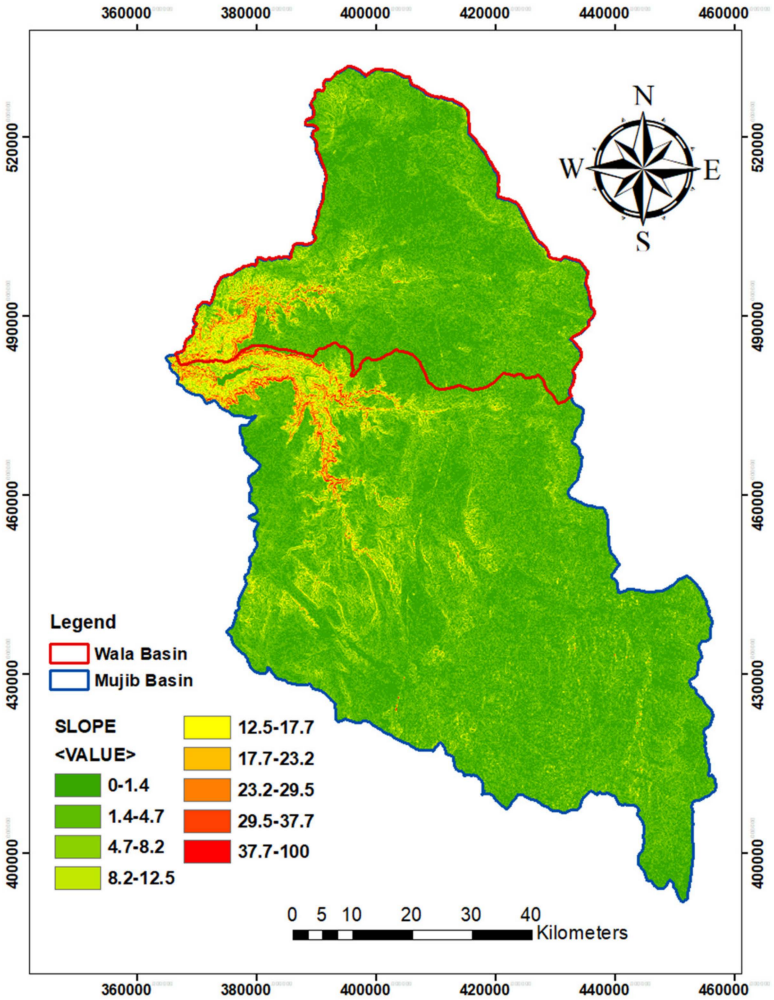


Figure 7. Slope map of Wadi Mujib.

Moving forward, this study introduced storms characterized by areal precipitation and runoff into the sophisticated HEC-HMS software to meticulously craft a hydrograph model. The calibration and validation phases constituted the cornerstone of the hydrological simulation, with temporal frameworks meticulously aligned to data availability. To ensure robust model performance, two-thirds of the available data were judiciously assigned to the calibration process, with the remaining third meticulously preserved for the rigorous validation phase. Furthermore, this study took into account a rainy day with a minimum rainfall depth of 0.1 mm, juxtaposed with the runoff values meticulously recorded at the stations, serving as representative metrics for average daily flow. This integrative and detail-oriented approach underscores the methodological rigor employed in unraveling the hydrological intricacies of the study area.

The calibration process involves the meticulous adjustment of the curve number (CN) values, particularly in relation to the initial estimates, while accounting for antecedent moisture conditions. This intricate calibration aims to refine the model's accuracy and align it closely with observed data. Notably, the calibration phase specifically targets the curve number, ensuring its optimal configuration for different antecedent moisture content scenarios. Figure 8 visually encapsulates the two-step calibration procedure, demonstrating

the dynamic adjustments made to enhance the model's predictive capabilities. In stark contrast, the validation phase refrains from any additional tuning or modifications to model parameters. Instead, it relies on a rigorous comparison between observed and simulated data generated by the catchment model. The correlation value (R2) assumes a critical role during this validation, serving as a quantitative metric to ascertain the ideal curve number values (CN). For instance, when the curve number is 78.5 at normal antecedent moisture content, the Pearson's coefficient registers at 0.8, indicative of a strong correlation. The nuances of these pivotal processes are intricately illustrated in Figure 8.

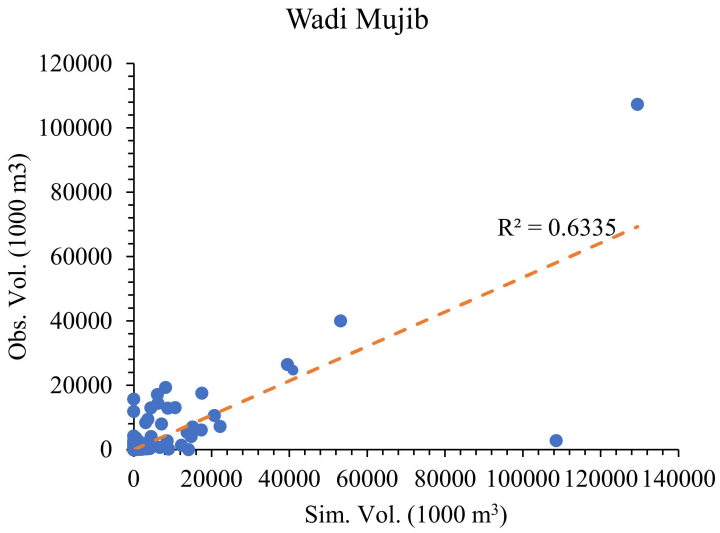


Figure 8. The observed data compared with simulated volume.

Shifting focus to rainfall data analysis, this study employed frequency analysis to statistically scrutinize the dataset. The coefficient of determination (R2) played a key role in identifying the most suitable distribution, with the General Extreme Value (GEV) distribution employed, plotted using the Weilbull formula. The comparison between actual and predicted rainfall exhibited a remarkably high coefficient of determination (R2) exceeding 0.99, attesting to the robustness of the chosen distribution model. This statistical foundation set the stage for determining the return period (2, 5, 10, 25, 50, and 100 years) of rainfall, offering a comprehensive perspective, illustrated in Figure 9 and detailed in Table 6. Expanding the analysis further, this study estimated flash flood flow at different return periods, enhancing our understanding of potential scenarios. Figure 10 and Table 7 comprehensively present the outcomes of these estimations, shedding light on the dynamic relationship between rainfall patterns and flash flood magnitudes under varying return periods. The thoroughness of this analytical framework underscores this study's commitment to unraveling the complexities of hydrological dynamics with precision and rigor.

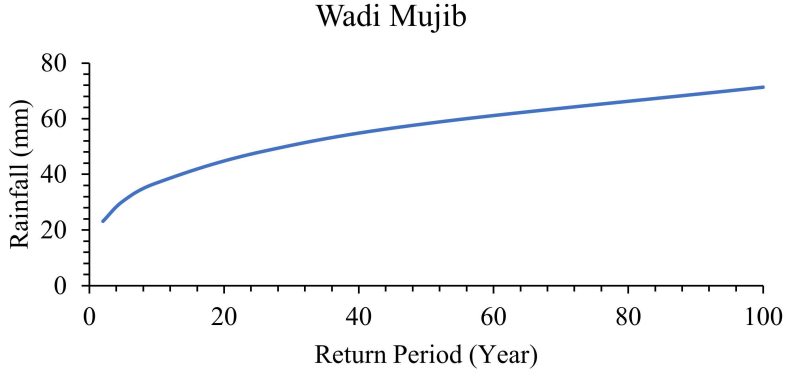


Figure 9. Return period of Wadi Mujib.

Table 6. The rainfall depth in mm at different return periods.

Return Period	2	5	10	25	50	100
Wadi Mujib	23.2	30.5	37	47.8	58.3	71.3

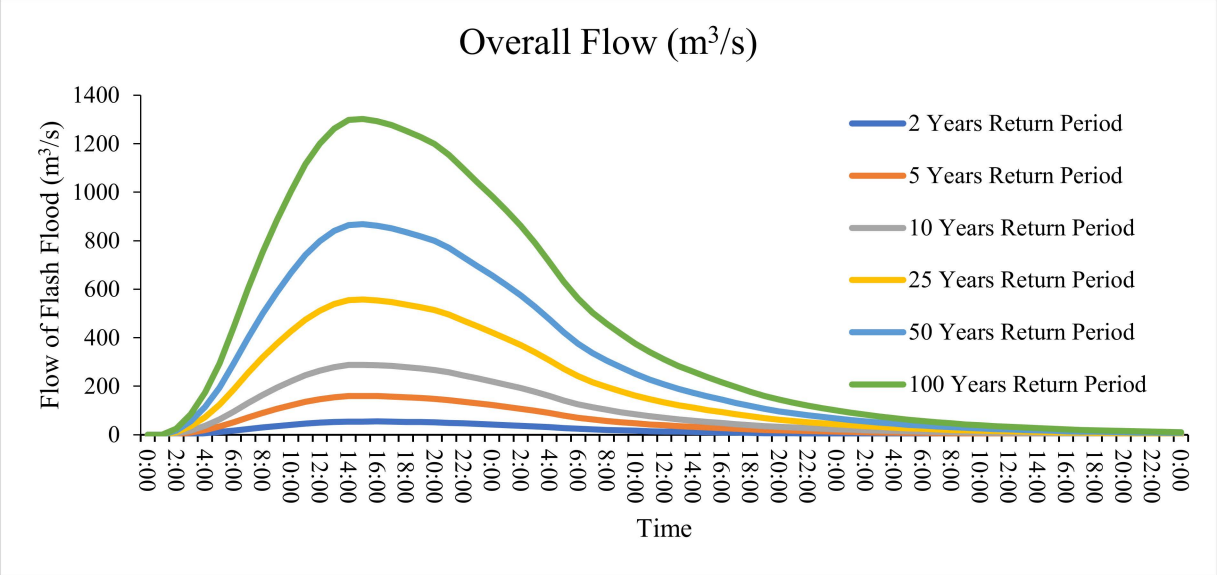


Figure 10. Flow of flash flood at different return periods.

Table 7. The rainfall and runoff depth in mm and peak flow in m^3/s at different return periods.

Return Period	2	5	10	25	50	100
Rainfall (mm)	23.2	30.5	37	47.8	58.3	71.3
Runoff depth in (mm)	1.09	3.19	5.75	11.1	17.29	25.94
Overall Peak Flow (m^3/s)	55	160.4	289	557.6	868.5	1303

Upon detecting substantial rainfall, the Flash Flood Potential Index (FFPI) emerges as a pivotal technique, offering a nuanced spatial assessment of hazard levels. This index draws on four primary physiographic parameters—slope, land use, plant cover, and soil texture [25]. Each parameter is meticulously categorized based on its susceptibility to flooding, laying the foundation for a comprehensive evaluation.

Leveraging the raster calculator feature within the ArcGIS software, the FFPI is determined through Equation (2), generating a detailed map encapsulating flash flood potential across Wadi Mujib. Figure 11 visually presents this map, highlighting potential locations with varying index values. Notably, the FFPI ranges from 1 (indicating the lowest potential) to 9 (representing the highest). This dynamic mapping approach provides a spatially explicit understanding of flash flood vulnerability.

The determination of the FFPI threshold, representing regions with the utmost potential for flash floods, is a critical step in the analysis. Setting the threshold at the 95% cumulative value in the basin plot ensures a focus on high-risk areas. This percentile is strategically selected based on the cumulative distribution of the basin. The attribute table of the FFPI map, exported to an Excel spreadsheet, facilitates precise calculations and delineation of areas corresponding to specific index values.

Figure 12 elucidates the 95th percentile threshold, showcasing a static trend at the chart's summit beyond this percentile. Through this method, it is established that the 95th percentile for the FFPI map is 7. This implies that areas with an index value of 7 or higher exhibit the highest flash flood potential. Quantitatively, this high-risk region

spans 575.12 km^2, constituting 13.39% of the total basin area, predominantly situated in the western part of the basin.

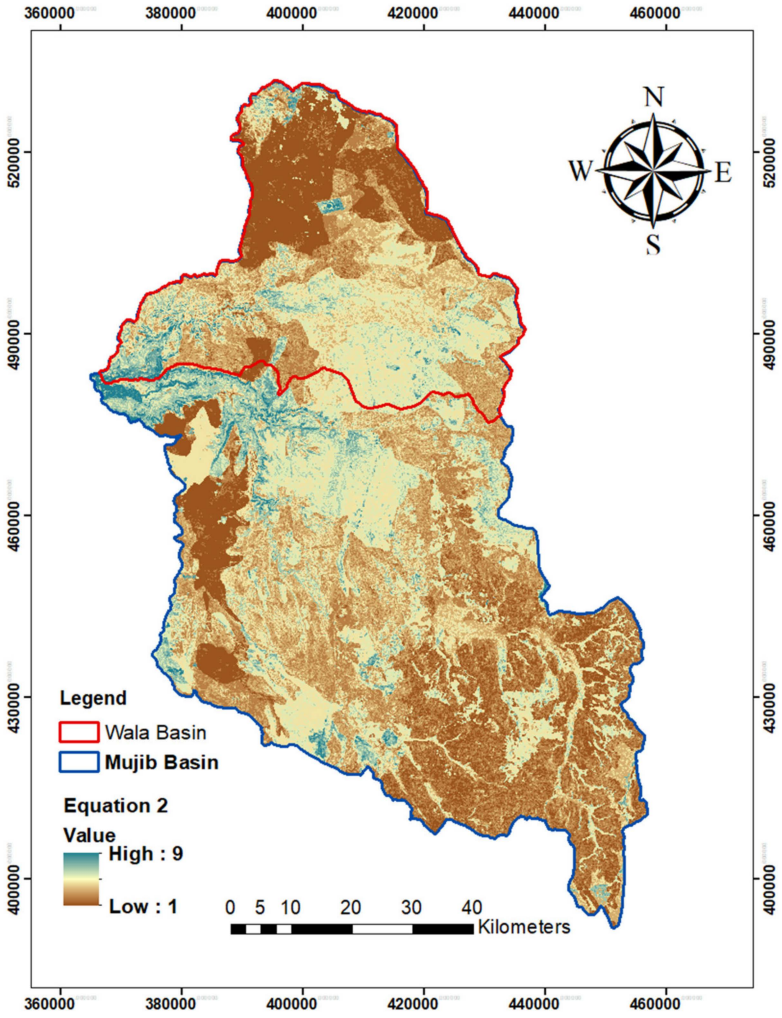


Figure 11. Flash flood potential map for Wadi Mujib.

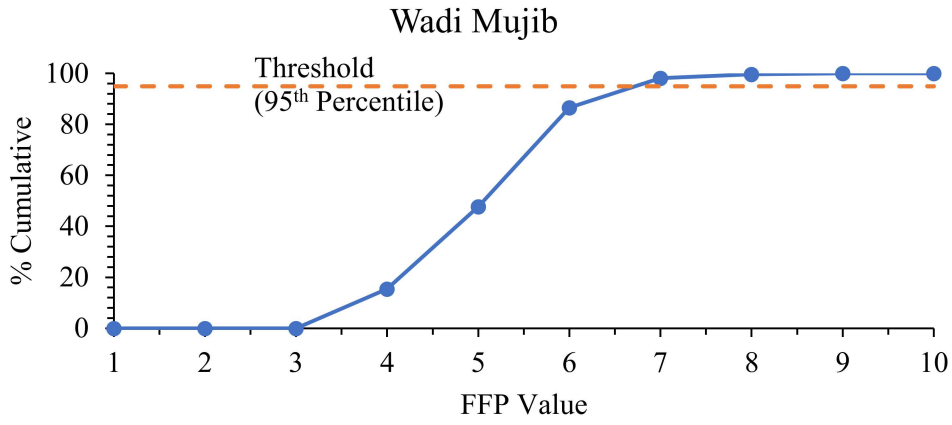


Figure 12. Cumulative curve of FFP value with the 95th percentile.

Further delving into the analysis, the percentage of hazard-prone areas classified as moderate (index values 5 and 6) encompasses 71.24% of the total basin area, totaling 3061.2 km^2. Conversely, the regions characterized by the lowest flash flood potential cover approximately 660.5 km^2, constituting 15.37% of the total area. This comprehensive spatial

assessment enhances our understanding of flash flood vulnerability, allowing for informed decision-making and mitigation strategies in the Wadi Mujib Basin.

4. Conclusions

In conclusion, flash floods pose a significant threat due to their intense and rapid nature, resulting in unpredictable high-flow velocities and catastrophic damage. Hydrological factors, particularly precipitation intensity and duration, play a critical role in flash flood occurrences. Urbanization and other factors contribute to the expansion of impervious surfaces, exacerbating flash flood risks.

The impact of climate change on flash floods in Jordan has contributed to the loss of both lives and property. Hydrological models like the curve number method have been extensively utilized to assess and predict flash floods. The integration of GIS environments and HEC-HMS software has played a significant role in enhancing hydrological modelling and the analysis of catchment parameters. Factors such as slope, land use, vegetation cover, and soil texture have been incorporated into flash flood potential maps using the FFPI method, enabling the identification of areas at high risk. This research study focused specifically on Wadi Mujib in Jordan and employed GIS and HEC-HMS software to simulate models. The Thiessen Polygon method was employed to quantify precipitation, while the HEC-HMS program facilitated hydrograph simulation. Calibration and validation processes were conducted using observed data and storm events. Frequency analysis was employed to examine rainfall data and estimate flash flood flows at different return periods. By utilizing the FFPI method, a flash flood potential map for Wadi Mujib was generated based on physiographic factors. The map depicted varying levels of flash flood potential, with the highest potential index recorded as 9 and the lowest as 1. The 95th percentile threshold was employed to identify regions with the highest potential for flash floods.

To sum up, this study provides valuable insights into the flash flood potential and magnitude in Wadi Mujib, Jordan. The integration of GIS and HEC-HMS software, coupled with the FFPI method, offers an effective approach for assessing and mapping flash floods. The findings contribute to a better understanding of flash flood risks and can aid in decision-making for flash flood warning systems. The study area's hydrological model can nevertheless simulate the peak flow of flash floods with good satisfactory accuracy, despite the challenges posed by the study area's lack of meteorological and hydrological data, and poor temporal and spatial resolution of land use and the soil map. Where the value of loss method in this study is 78.5 as curve number (CN) method. In addition, on flash flood potential map for the selected basin, the highest FFPI is around 13.39%, with moderate potential of 71.24% and low potential of 15.37%. High FFPI areas are characterized by low vegetation cover, bare rock and soil, or urban areas. As a result, it might be dangerous to people or their property. In order to reduce the risks of flash floods that endanger human lives and their property, both structural and non-structural measures should be put in place.

Author Contributions: Methodology, M.S.; Conceptualization, M.S. and F.A. (Fares AlMomani); Data curation, M.S., Y.A., A.A. and F.A. (Fayez Abdullah); Funding acquisition, M.S. and F.A. (Fares AlMomani); Supervision, A.-S.A.O. and F.A. (Fares AlMomani); Software, Y.A. and A.A.; Validation, M.S., Y.A., A.A. and F.A. (Fayez Abdullah); Investigation, Y.A., A.A. and F.A. (Fayez Abdullah); Resources, A.-S.A.O. and F.A. (Fares AlMomani), A.A.; Writing—original draft, M.S. and A.-S.A.O.; Writing—review & editing, H.H.A. All authors have read and agreed to the published version of the manuscript.

Funding: This research was funded by Ministry of Higher Education and Scientific Research in Jordan, grant number WE/1/5/2021. Open Access funding provided by the Qatar National Library.

Data Availability Statement: The data presented in this study are available on request from the corresponding author.

Acknowledgments: The authors are immensely thankful to the Scientific Research and Innovation Support Fund in the Ministry of Higher Education in Jordan for their support of the project numbered

WE/1/5/2021 entitled "Flood early warning system: design, implementation and computational modules in Mujeb basin/Jordan". Their commitment to promoting scientific research has profoundly impacted our work, and we are honored to be a beneficiary of their support.

Conflicts of Interest: The authors declare no conflict of interest.

References

1. Dawod, G.; Hossain, F.; Hasan, S.; Shamseldin, A.Y. Application of HEC-HMS and GIS in flood forecasting of El-Mina drainage basin, Tripoli, Lebanon. *J. Geogr. Inf. Syst.* **2011**, *3*, 273–285.
2. Elkhrachy, I. Assessing flash flood hazard using GIS-based multi-criteria analysis in Wadi El-Natrun, Egypt. *J. Earth Sci. Clim. Chang.* **2015**, *6*, 1–7.
3. Azmeri, A.; Hoque, M.A.; Adham, M.I.; Khandaker, M.U. Flood modeling using HEC-HMS and GIS: A case study of Surma River basin, Bangladesh. *Int. J. Geosci.* **2016**, *7*, 780–792.
4. El Alfy, M.A. Hydrologic modeling of a desert wadi using HEC-HMS and GIS techniques. *Appl. Water Sci.* **2016**, *6*, 111–121.
5. United Nations Framework Convention on Climate Change (UNFCCC). Jordan's Third National Communication. 2014. Available online: https://unfccc.int/sites/default/files/resource/jdrnc3.pdf (accessed on 29 September 2023).
6. Shawaqfah, M.; Almomani, F.; Khatatbeh, A. Mapping Flash Flood Potential and Risk Level Using GIS Techniques and the Flash Flood Potential Index (FFPI) in Amman Zarqa Basin of Jordan. *Jordanian J. Eng. Chem. Ind. (JJECI)* **2020**, *3*, 64–73. [CrossRef]
7. Mandal, S.; Chakrabarty, D. Hydrological modeling of a river basin using HEC-HMS and GIS. *Model. Earth Syst. Environ.* **2016**, *2*, 1–14. [CrossRef]
8. Javelle, P.; Gallart, F. Runoff generation processes in an urbanized catchment: Claise catchment (Tours, France). *J. Hydrol.* **2010**, *394*, 177–188.
9. Georgakakos, A.; Lall, U.; Ntelekos, A.; Foufoula-Georgiou, E.; Ding, D. A GIS-integrated system for flash-flood prediction. *J. Hydrol.* **1997**, *198*, 269–299.
10. Sweeney, J.M.; Baumgardner, T.R. Flash flood forecasting: An ingredients-based methodology. *Weather. Forecast.* **1999**, *14*, 547–567.
11. Arachchige, S.P. An integrated GIS and multi-criteria decision-making technique for flash flood susceptibility assessment. *J. Hydroinform.* **2015**, *17*, 955–973.
12. Arachchige, D.R. *Mapping Flash Flood Potential Using GIS and the Flash Flood Potential Index (FFPI) in the Turtle River and Forest River Basin s in North Dakota*; University of North Dakota: Grand Forks, ND, USA, 2015.
13. Azmeri Hadihardaja, I.K.; Vadiya, R. Identification of flash flood hazard zones in mountainous small basin of Aceh Besar Regency, Aceh Province, Indonesia. *Egypt. J. Remote Sens. Space Sci.* **2016**, *19*, 143–160.
14. JICA/WAJ (Japan International Cooperation Agency/Water Authority of Jordan). *Hydrologeological and Water Use Study of the Mujib Watershed, Appendix (I)*; Final Report; JICA/WAJ: Amman, Jordan, 1987.
15. Brewster, J. The Flash Flood Potential Index for WFO Binghamton NY. 2004. Available online: http://bgmresearch.eas.cornell.edu/research/ERFFW/presentations/june_02_2010/Brewster_Jim_Development_of_FFPI.ppt (accessed on 20 December 2019).
16. Dawod, G.M.; Mirza, M.N.; Al-Ghamdi, K.A. GIS-Based Spatial Mapping of Flash Flood Hazard in Makkah City, Saudi Arabia. *J. Geogr. Inf. Syst.* **2011**, *3*, 225–231. [CrossRef]
17. El Alfy, M. Assessing the impact of arid area urbanization on flash floods using GIS, remote sensing, and HEC-HMS rainfall–runoff modeling. *Hydrol. Res.* **2016**, *47*, 1142–1160. [CrossRef]
18. Elkhrachy, I. Flash Flood Hazard Mapping Using Satellite Images and GIS Tools: A case study of Najran City, Kingdom of Saudi Arabia (KSA). *Egypt. J. Remote Sens. Space Sci.* **2015**, *18*, 261–278. [CrossRef]
19. Kruzdlo, R. Flash Flood Potential Index for the Mont Holly Hydrologic Service. 2010. Available online: http://www.state.nj.us/drbc/library/documents/Flood_Website/flood-warning/user-forums/Krudzlo_NWS.pdf (accessed on 20 December 2019).
20. Mandal, S.P.; Chakrabarty, A. Flash flood risk assessment for upper Teesta river basin: Using the hydrological modeling system (HEC-HMS) software. *Model. Earth Syst. Environ.* **2016**, *2*, 59. [CrossRef]
21. Minea, G. Assessment of the flash flood potential of Bâsca River Catchment (Romania) based on physiographic factors. *Open Geosci.* **2013**, *5*, 344–353. [CrossRef]
22. Gokceoglu, C.; Aksoy, H.; Keskin, I. Multivariate statistical analysis for flood triggering conditions in the eastern Black Sea region of Turkey. *Hydrol. Process.* **2011**, *25*, 1393–1403.
23. Smith, G.E. Flash Flood Potential: Determining the Hydrologic Response of FFMP Basins to Heavy Rain by Analyzing Their Physiographic Characteristics. 2003. Available online: http://www.cbrfc.noaa.gov/papers/ffp_wpap.pdf (accessed on 20 December 2019).
24. Smith, D.I. Flash flood potential index (FFPI): Development and verification. *Hydrol. Earth Syst. Sci.* **2010**, *14*, 763–774.
25. Pathirana, A.; Radhakrishnan, M.; Malmgren-Hansen, D. A review of rainfall–runoff models for urban catchments: Urban flood mitigation and climate change perspectives. *Environ. Rev.* **2015**, *23*, 414–429.
26. Sposito, G. *The Chemistry of Soils*; Oxford University Press: Oxford, UK, 2008.
27. Al-Sa'ed, R.; Abu Shqair, H. Flash flood hazard assessment and mapping in Jordan using GIS and multi-criteria decision analysis. *Geomat. Nat. Hazards Risk* **2018**, *9*, 420–437.

28. Azmeri, A.; Bari, S.; Shahid, S.; Nath, B. Flash flood susceptibility assessment and mapping using GIS-based multi-criteria decision analysis: A case study of the Buriganga River Basin, Bangladesh. *Nat. Hazards* **2017**, *89*, 227–250.
29. Al-Ansari, N.; Knutsson, S. Flash flood prediction using remote sensing and GIS in arid areas: A case study in Jordan. *J. Environ. Hydrol.* **2014**, *22*, 1–10.
30. Al-Ansari, N.; Knutsson, S. Flash flood analysis and hazard mapping using GIS and HEC-HMS in Wadi Al-Arab Dam, Jordan. *J. Earth Sci. Geotech. Eng.* **2015**, *5*, 47–64.
31. Al-Ansari, N.; Knutsson, S. Flash flood potential assessment in arid areas using remote sensing, GIS, and HEC-HMS: A case study in Wadi Al-Namlah, Jordan. *Water Resour. Manag.* **2016**, *30*, 935–950.
32. Dawod, G.; Al-Ansari, N.; Knutsson, S. Flash flood potential mapping using GIS and remote sensing techniques in Upper Citarum Basin, West Java, Indonesia. *J. Flood Risk Manag.* **2013**, *6*, 145–158.
33. Elkhrachy, I. Integration of multi-criteria decision analysis and GIS for flash flood susceptibility mapping: A case study of Sharm El-Sheikh, Sinai Peninsula, Egypt. *Nat. Hazards* **2017**, *87*, 59–80.
34. Zogg, J.; Deitsch, K. The Flash Flood Potential Index at WFO Des Moines, Iowa. 2013. Available online: http://www.crh.noaa.gov/images/dmx/hydro/FFPI/FFPI20WriteUp.pdf (accessed on 20 December 2019).
35. Digital Elevation Model (DEM) of 30 m Was Downloaded from USGS Earth Explorer. Available online: https://earthexplorer.usgs.gov/ (accessed on 25 April 2023).
36. U.S. Geological Survey (USGS). Earth Explorer. 2018. Available online: https://earthexplorer.usgs.gov (accessed on 20 December 2019).
37. Chen, C.T. Extensions of the TOPSIS for group decision-making under fuzzy environment. *Fuzzy Sets Syst.* **2000**, *114*, 1–9. [CrossRef]
38. Ministry of Agriculture (MOA). Ministry of Agriculture: Amman, Jordan. 1993. Available online: https://moa.gov.jo/Default/EN (accessed on 20 December 2019).
39. Smith, E.G. *Development of a flash Flood Potential Index Using Physiographic Datasets within a Geographic Information System*; University of Utah: Salt Lake City, UT, USA, 2010.
40. Jansen, L.J. GIS-based hydrologic modeling of a semi-arid basin: The Upper San Pedro, Arizona. *J. Hydrol.* **2003**, *275*, 147–165.
41. Kiani Chapeleh, A.; Homaee, M.; Ghahraman, B. Integration of remote sensing and GIS for flash flood susceptibility assessment: A case study in Iran. *Nat. Hazards* **2014**, *70*, 1419–1438.
42. Lin, C.H.; Hong, N.M.; Chen, C.F. Integrating geographic information systems and support vector machines for the assessment of flood potential areas in Taipei. *Comput. Geosci.* **2008**, *34*, 837–845.
43. Mandal, A.; Chakrabarty, D. Flood mapping and inundation prediction using GIS and hydrodynamic modeling: A case study of the Mahananda River Basin, India. *Geomat. Nat. Hazards Risk* **2017**, *8*, 1359–1382.
44. Masoud, M.A.; Su, Z. Flash flood forecasting using artificial neural networks: An overview and methodology. *J. Hydrol.* **2008**, *349*, 355–365.
45. Nguyen, L.T.; Saghafian, B. Flash flood inundation mapping using a hydraulic model coupled with a geospatial model. *Nat. Hazards* **2016**, *81*, 241–257.
46. Sharma, T.C.; Ojha, C.S.P.; Kumar, V.; Sharma, P. Hydrological modeling of a small basin using HEC-HMS: A case study of Gokyo Basin, Nepal. *J. Water Clim. Change* **2017**, *8*, 42–54.
47. Tsai, M.H.; Chen, L.C.; Chang, T.J. Analysis of flood patterns using GIS and remote sensing. *J. Hydrol.* **2005**, *311*, 49–62.

Disclaimer/Publisher's Note: The statements, opinions and data contained in all publications are solely those of the individual author(s) and contributor(s) and not of MDPI and/or the editor(s). MDPI and/or the editor(s) disclaim responsibility for any injury to people or property resulting from any ideas, methods, instructions or products referred to in the content.